ACTIVE MAGNETIC BEARINGS USED IN BW/IP CENTRIFUGAL PUMPS

K. Pottie, G. Wallays, J. Verhoeven, R. Sperry
BW/IP International B.V., Etten-Leur, The Netherlands
L. Gielen, D. De Vis
LMS International, Leuven, Belgium
T. Neumer, M. Matros
University of Kaiserslautern, Kaiserslautern, Germany
R. Jayawant
Glacier RPB, Shoreham by Sea, Great Britain

ABSTRACT

Prediction of the dynamic behaviour of pump rotors requires a profound knowledge of fluid excitation and motion dependent forces on all rotor components. In order to characterize these forces at the impellers, a test rig was built, in which a multistage boilerfeed pump is suspended in active magnetic bearings (AMB). External signals fed into the electronic controller of the AMB excite the rotor following well defined orbits.

Force and displacement measurements at the bearings provide on-line FRF's which are the basis for identification of fluid forces, for health monitoring / diagnostics, and for modal analysis.

This paper describes the AMB's and the control loop. Two excitation techniques are briefly discussed. The parameters characterizing the dynamics of the AMB's are identified. They are related to the lay out of the electro magnets and the electronic controller. Extensive calibration of the magnetic forces was necessary to generate correct FRF's. Finally, some motion dependent forces acting on an impeller are shown. These forces are obtained from the FRF's in combination with an indirect identification technique on the flexible pump rotor.

1 INTRODUCTION

Fluid / structure interaction forces of annular clearance seals and impellers are dominating factors in the dynamic behaviour of large multistage boilerfeed pumps (BFP).

These forces can be divided into two groups:

a. Pure hydraulic forces, generated by the pumping action of the impellers.

b. Motion dependent interaction (MDI) forces generated by the vibrations of the BFP rotor. The vibrations may often be considered as perturbations around the static equilibrium of the rotor. The MDI-effects can then be linearized (eventually over a certain frequency range) and modelled by equivalent mass, stiffness and damping matrices, relating forces and moments to the corresponding radial, angular and axial displacements (fig. 1). The diagonal coefficients are called "direct", the other coefficients are "cross coupled".

The Brite Euram - BE-3472-89 - research project in which an AMB suspended boilerfeed pump is used was mainly set up to quantify both types of interactions on impellers. The theory of identifying MDI forces is described more profoundly in [2] and [4]. It is based on frequency response functions (FRF) between externally applied excitation forces and resulting shaft displacements, over a frequency range from zero to multiple times rpm. Because the impellers / seals of the flexible BFP rotor aren't accessible during operation a high quality rotor dynamic model and inverse matrix operations are necessary to relate the measurements at the bearings with fluid effects at impellers / seals.

In the same project a single stage process pump at the University of Kaiserslautern is used to identify hydraulic and MDI forces on impellers and long annular seals. This component test rig is also

suspended by AMB. The forces are quantified using FRF techniques as well. Since this pump rotor is rigid, forces and displacements can be related by simple geometrical relations.

2 REQUIREMENTS IMPOSED BY THE MULTISTAGE BOILERFEED PUMP TEST RIG

The magnetic bearings and control system are designed to the following requirements:

1. Suspension capabilities: Static loads are 2000 N maximally. Estimations are based on deadweight and static impeller forces. The dynamic loads are specified per frequency (table 1). Loads were extracted from [7], [8].

TABLE 1: Bearing loads boilerfeed pump

BW/IP Byron Jackson Boilerfeed Pump - Type HDB

Size	:	8x10x14, up to seven stages
Power	:	Up to 5 MW
Test Speeds	:	Up to 3000 RPM

Radial Loads
Static (max)	:	2000 N

Maximum Dynamic Pump Operating Loads at 3000 RPM
Low frequency	:	750 N
1x Rotation	:	2450 N
Vane Passing	:	1450 N
Random	:	500 N

Thrust Loads
Static Loads	:	2000 N momentary up to 4000 N
Dynamic Loads	:	1500 N max at 3000 RPM

2. Rotor stability requirements: multilobe or tilting pad hydro dynamic bearings used in conventional boilerfeed pumps generate high direct stiffness ($2 \cdot 10^8$ N/m) and damping effects, and minimal cross coupled stiffness and damping. All these coefficients are benign for the rotor stability.

Modelling the dynamics of the AMB supported rotors revealed that equivalent bearing stiffnesses of two orders of magnitude lower have acceptable influence on the 2nd and 3rd mode and no drastic change on the first mode. Equivalent damping coefficients however had to meet following values for stable operating conditions:

2 stage rotor	18000 Ns/m
7 stage rotor	60000 Ns/m

Cross coupling between orthogonal excitation directions was kept minimal by mounting auxiliary coils, eliminating leakage fluxes, in between the principal coils. The auxiliary coils also provide significantly more ampère turns.

3. Excitation capabilities: as the operating rotor is subjected to artificial excitations, additional forces on top of the normally occurring bearing loads are required. Displacements must be sufficiently high to obtain good measurement accuracy. On the other hand displacements must remain about 20% of the radial clearances of the BFP rotor. The latter condition is necessary for linearization of the MDI effects. Fig. 2 and 3 list the desired force and displacement spectrum.

4. Avoidance of disturbance of cross coupled fluid dynamic coefficients. This is the main reason for eliminating cross coupling between the AMB as much as possible. Exciting the rotor in x direction creates cross coupled fluid force and displacement in y-direction. A leakage flux generates an additional direct coupled fluid force and displacement in y direction. It would be impossible to separate direct coupled from cross coupled fluid effects.

5. Sensitivity considerations: the error sensitivity of the indirect fluid / structure interaction identification technique, with respect to both measurement as rotor model errors, can be mitigated using AMB with high damping values.

6. Stable coast down when stopping. Emergency coast down: in case of instabilities causing uncontrolled rotor displacements, power is switched off and the rotor runs out on dry lubricated bushings. The latter are designed for 10 emergency stops.

7. Water temperatures of 150°C. The transducer sensors and transducer local amplifiers must be cooled in order to maintain high accuracy.

Further on, displacement and velocity sensors, as well as the forces generated by the AMB must be correct for generation of high quality FRF. Therefore it was specified:

- accuracy of all amplitudes within 1%
- phase shift within 5°

3 CONTROL LOOP

Fig. 3 represents the controller scheme of the AMB. The position of the shaft and the rate of change of position are measured independently one from the other. A well defined disturbance signal is applied for excitation of the rotor. Each signal is fed into a separate block.

Direct measurement of the velocity signal improves the accuracy, compared with derivation of the position signal. Time delays are eliminated.

The output of these blocks is combined with a bias current, to increase stiffness (fig. 4). This signal is input to the drive circuits of the pulse width modulation power amplifier. Tight current feedback compensation insures that the AMB current is proportional to the input signal of the power stage, over a range of frequencies up to 2 kHz.

Measurements of the electro magnetic currents and of the displacements allow a force card to generate the corresponding magnetic force signals. Extensive calibrations are necessary to establish a correct relationship between airgaps, currents and forces.

For every bearing degree of freedom, a set of two radial diametrically opposed displacement and two radial diametrically opposed velocity sensors is installed, in order to mitigate the effect of mechanical run out. This sensor configuration is applied at each end of each radial bearing. The signals are used to calculate displacement / velocity in the point of application of the magnetic force. Such complex lay out is necessary because the rotor behaves flexible in large L/D AMB.

Direct measurements of the bearing forces and responses allow to consider the rotor as a free body on which the AMB exert excitation forces. It is not necessary to model the AMB in terms of equivalent stiffness and damping to obtain rotor FRF's during excitation. As such, fluid / rotor identifications become completely independent from the control loop and AMB parameters.

4 FORCE CALIBRATION

Each radial magnetic bearing consists of two diametrical coils. The resultant load in x or y direction is described by

$$F_{net} = \frac{\mu_o \cdot N^2 \cdot S}{8} \left[\frac{(I_{o1} + \Delta I_1)^2}{(\varepsilon_{o1} + \Delta \varepsilon)^2} - \frac{(I_{o2} + \Delta I_2)^2}{(\varepsilon_{o2} - \Delta \varepsilon)^2} \right] \quad (1)$$

Bearing currents I_1, I_2 and airgaps ϵ_1, ϵ_2 contain two contributions. The first component is related to the position of the non-excited shaft. The second component $\Delta\epsilon$ describes the change due to the artificial excitation of the rotor. S is a factor, mainly related to the flux surface. μ_o is the magnetic permeability, N the number of windings.

To take into account the individual physical properties of each coil and control loop, eq. (1) was replaced by:

$$F_{net} = K_1 \left(\frac{I_{01} + \Delta I_{01}}{\varepsilon_{01} + \Delta \varepsilon} \right)^{e_1} - K_2 \cdot \left(\frac{I_{02} + \Delta I_2}{\varepsilon_{02} + \Delta \varepsilon} \right)^{e_2} \quad (2)$$

with $e_1 \sim e_2 \sim 1.8$, for the radial bearings.

To verify the accuracy of the calculated forces over a wide load range, the non rotating and dry shaft was loaded by a tuneable stiff ground connection, in which the force was measured by a precision load cell. Equilibrium equations allowed to verify the AMB forces. Three major errors appeared when using the force model of equation 2:

- Dependency of calculated force output on rotor position (fig. 5)
- Dependency of calculated force output on the load. The error is linear for low loads, and non linear for high loads.
- Hysteresis effects: when a cyclic external load is applied, a different force error value is found for each load value, depending on this load being increasing or decreasing. Further on, the force error is higher for upward shaft displacements than for downward (fig. 6).

The calibration constants in eq. (2) are only slightly affected by shaft position, but differ for different external load directions and for different load signs.

To cope with some of the force errors, a large number of external load conditions were applied for a number of different shaft positions, resulting in a force error matrix. The latter provides design data for a hardware correction, which allows a tuneable linear adjustment of force output with the original force output value, the position information and a DC offset value, independent for each bearing degree of freedom.

As all previous corrections were based on DC

calibration, another series of measurements was made to investigate the influence of residual and hysteresis phenomena on the AC force output:

- Linearity check
  AMB - FRF are measured for different input levels, with a max. / min. ratio higher than 4. All FRF are very similar (fig. 7), for frequencies higher than 20 Hz. Bad coherences occur below 20 Hz, especially at low input levels.

- Mass identification was possible from the axial FRF using axial AMB excitation. The rotor is considered stiff in axial direction.

- Comparison of analytical and measured FRF by hammer excitation on one hand (performed on the rotor while suspended in flexible slings) with the measured FRF by broadband AMB excitation on the other hand (performed on the dry and non rotating rotor) (fig. 8).

- Based on the measured displacements and on the numerical transfer function matrix for the dry and non-rotating rotor, the excitation forces are calculated and compared to the direct force measurements. The results of this experiment include all deviations related to:

  - Force measurement accuracy
  - Displacement measurement accuracy
  - Analytical model accuracy

  For frequencies below 20 Hz and for very low force levels, deviations of up to 50% are found.

Mass identification from radial FRF by AMB excitation was impossible because of the flexibility of the rotor.

From all these tests it was concluded that the modifications made to the force signal output section, improved the accuracy to a degree that for frequencies higher than 20 Hz it was impossible to make a distinction between AMB force error and other measurements or model error.

5 SHAFT EXCITATION METHODS

Two excitation techniques were considered: broad band vs. stepped sine. The approach of each excitation consists of the accumulation of auto- and crosspower spectra of all displacement signals and the excitation forces, followed by the estimation of the corresponding set of FRF's.

For sinusoidal excitation the different spectra are built frequency per frequency. At each frequency new time histories are measured and the fundamental signal component corresponding to the excitation frequency is retained. This is different to broad band excitation, where the spectra are obtained as a whole by means of the FFT transformation of the acquired time histories.

Although the frequency per frequency approach of stepped sine testing is considerably slower than for broad band testing, the major advantage is that an important noise reduction is obtained. This is because the low spectral density of broad band signals at low frequencies is eliminated.

Also traditional signal processing errors associated with the spectral analysis of broad band signals, such as leakage, can be completely avoided.

Fig. 9 compares stepped sine FRF with broadband FRF. A clear improvement of the FRF quality below 30 Hz can be observed. In general, the concentration of all excitation energy at one single frequency resulted in a force level increase of a factor 25. Displacements of up to 50 μm peak are measured. The resulting coherence is very high over the full frequency range.

When multiple inputs are used for 5 DOF identifications, these must be uncorrelated to allow correct calculation of FRF with respect to all inputs. The force signals showed to be far more uncorrelated than the displacement signals, and therefore were defined as inputs. Proper selection of the force sets results in maximal information on the dynamic rotor behaviour.

Fig. 10 lists the applied force sets. Each set is defined by a relative amplitude and phase angle with respect to the "first" force. To allow a 5x5 MDI matrix, axial excitation is added. FW refers to a forward whirling force, BW to backward whirling.

6 OPERATIONAL MEASUREMENTS

Fig. 11 shows amplitude spectra for a bearing force and a proximity probe with and without artificial broad band excitation. The upper graphs correspond to 2950 rpm while the lower graphs are measured at 1900 rpm. It can be seen that in the worst case a non synchronous vibration level difference of 1 decade is reached.

7 AMB CHARACTERISTICS

The availability of both force and displacement information at each bearing allows to estimate the AMB characteristics from measured AMB - FRF. Fig. 12 shows equivalent stiffness and damping coefficients of a radial bearing. These values depend on the electro magnets, on the settings of the control loop and also on the static load and the bias airgap. The coefficients are obtained by stepped sine excitation on a dry and non-rotating shaft.

Both stiffness (real part of the AMB - FRF) as damping (imaginary part of the AMB - FRF) change with frequency. Damping drops off very fast with decreasing frequency. At frequencies below $\pm$ 20 Hz, negative values are found. The asymptotic values for higher frequencies (> 40 Hz) are close to the minimal values specified by BW/IP. The radial bearing stiffness values are about $15 \cdot 10^6$ N/m which is an order of magnitude higher than expected.

The complex stiffness can be approximated by

$$K = k + j \cdot \omega \cdot c + I/j\omega$$

where k = stiffness of AMB
c = 'asymptotic' damping of AMB
I = correction factor, calculated from $\omega_0 = \sqrt{I/c}$, with ω_0 the zero crossing frequency of the damping.

Measurements showed that the frequencies at which the integration action of the PID controller equals its derivative action, correspond very well with ω_0. Identification of the parameters of the PID controller did not reveal any time delay in the frequency zone of interest.

The impedance of the AMB coil generates a single pole. No other dynamic effects are introduced by the electronic components between the PID output and the AMB current. The pole frequency is above the frequency range of 200 Hz. Nevertheless, the smooth decrease of damping - at higher frequencies - can be related to this pole. The increase of stiffness with increasing frequency can be explained partially as well.

Further on the increase of stiffness with frequency can be related to a measured frequency and load dependent drop off and phase shift for the displacement and velocity signals. As displacement information is used for P action and velocity signals for derivative action, this phase shift propagates through the controller,

contaminating K.
The disturbances of the displacement and velocity sensors (see also chapter 4) are probably caused by leakage fluxes of the electro magnets into the sensors.

Fig. 12 also suggests a resonance occuring at approximate 5 Hz. Since the dry rotor behaves free-free (no rigid body motion eigenfrequencies) in the AMB, the resonance of fig. 12 might be caused by amplitude / phase errors or non linear behaviour that can introduce important errors in the AMB - FRF.

8 IDENTIFICATION OF FLUID FORCES

Fig. 13 shows the indirectly identified MDI forces of a single centrifugal impeller, whirling on a circular orbit. The forces are applied in radial and tangential direction. They are made non dimensional according to [10].

The frequency range was limited from 5 to 65 Hz. The upper limit is because important casing resonances occurred at higher frequencies. As the measured FRF are compensated to mitigate the resonance effects assuming there is no fluid coupling between rotor and stator, and as none of the fluid models take into account independent DOF motions of the casing, the identified MDI forces for frequencies higher than 65 Hz are probably inaccurate.

These results suggest it is possible to identify fluid forces in impellers / seals, and to develop diagnostics on basis of on-line FRF, using inverse methods.

9 CONCLUSION

The test rig proves that it is possible to suspend large boilerfeed pump rotors in active magnetic bearings. Furthermore, AMB's can be used as exciters. Several exciter patterns are possible. FRF between on-line measured magnetic forces and displacements can potentially be used:

- To identify fluid forces in impellers / seals, in combination with inverse methods.
- To perform diagnostics, especially in combination with rotor complex modal parameter estimation techniques.

A crucial condition is that both response and AMB magnetic forces are of high quality to yield accurate FRF's. Here still some progress has to be made, especially at lower frequencies.

Another major restraint for diagnosis is that deteriorating rotor properties such as increasing wearring and impeller tip clearances must show up in the FRF in order to be identifiable.

REFERENCES

1. Verhoeven, J.J., De Vis, D., Nordmann, R., "Development and Operating Experience of a 5000 kW Test Boilerfeed Pump on Active Magnetic Bearings", International Conference on Power Station Pumps and Fans, 12-13 May 1992, IMechE London

2. Verhoeven, J.J., De Vis, D., Gielen, L., "Indirect Prediction of Internal Forces and Displacements in a full scale Boilerfeed Pump", 15-17 July 1992, Senlis France

3. Sperry, R.K., Verhoeven, J.J., "Improved Diagnostics of Main Coolant Pumps using Artificial Excitation", EPRI International Main Coolant Pump Seminar, August 1993, Toronto

4. Verhoeven, J.J., "Identification of Fluid / Structure Interaction for the Development and Design of Boilerfeed Pumps", Final Technical Report of Brite Euram Program BREU-102-C, July 1993

5. Nordmann, R., Verhoeven, J.J., De Vis, D., "Identification of Fluid / Structure Interaction in Centrifugal Pumps (Part 2: experimental results)", ISROMAC 4, April 5-9, 1992 Honolulu, Hawaii USA

6. Knight, J.D., Xia, Z., McCaul, E., Hacker, H.Jr., "Determination of Forces in a Magnetic Bearing Actuator: Numerical Computation with Comparison to Experiment", Journal of Tribology, October 1991

7. Verhoeven, J.J., "Unsteady Hydraulic Forces in Centrifugal Pumps", Int. Conf. IMechE, Part Load Pumping Operations, Control and Behaviour, Heriot-Watt Univ., Edinburgh, UK (Sept. 1-2, 1988)

8. Bolleter, U., Wyss, A., Welte, I., Stüchler, R., "Measurement of Hydrodynamic Interaction Matrices of Boilerfeed Pump Impellers", Transaction of the ASME, Vol. 109, April 1987

9. Keith, F.J., Maslen, E.H., Humphris, R.R., Williams, R.D., "Switching Amplifier Design for Magnetic Bearings", 2nd International Symposium on Magnetic Bearings, Tokyo, July 12-14, 1990

10. Ohashi, H., Shoji, H., "Lateral Fluid Forces acting on a Whirling Centrifugal Impeller in a Vaneless Diffusor", 3rd Workshop on Rotor Dynamic Instability Problems in High Performance Turbo Machinery, Texas A&M University, May 1984
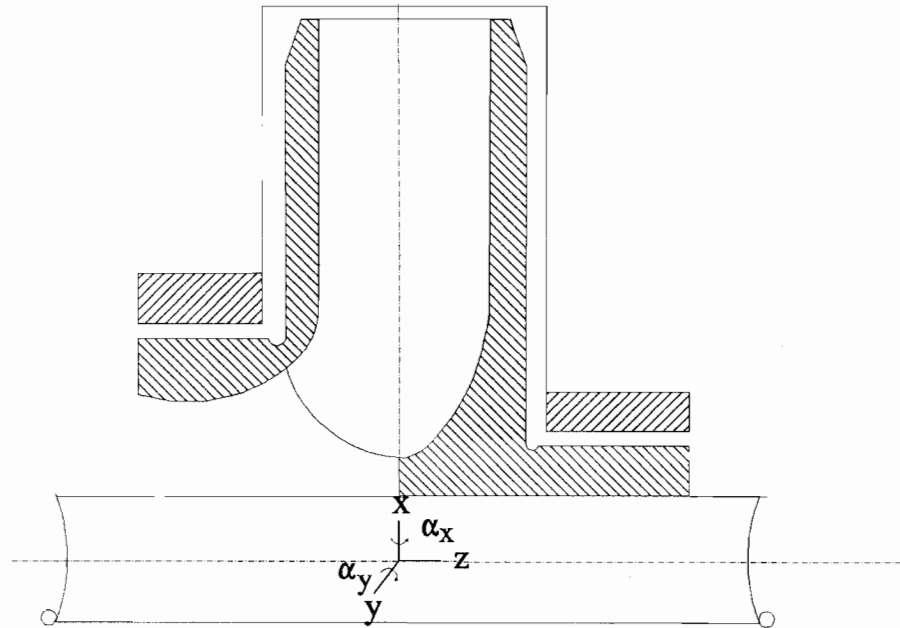
$$
\begin{bmatrix} F_x \\ F_y \\ M_y \\ M_x \\ F_z \end{bmatrix} = \begin{bmatrix} M & m & M_{e\alpha} & -m_{e\alpha} & M_{ez} \\ -m & M & -m_{e\alpha} & -M_{e\alpha} & M_{ez} \\ M_{\alpha e} & m_{\alpha e} & M_\alpha & -m_\alpha & M_{e\alpha} \\ m_{\alpha e} & -M_{\alpha e} & m_\alpha & M_\alpha & m_{e\alpha} \\ M_{ze} & m_{ze} & M_{z\alpha} & m_{z\alpha} & M_z \end{bmatrix} \begin{bmatrix} \ddot{X} \\ \ddot{Y} \\ \ddot{\alpha}_y \\ \ddot{\alpha}_x \\ \ddot{Z} \end{bmatrix}
$$

$$
+ \begin{bmatrix} C & c & C_{e\alpha} & -c_{e\alpha} & C_{ez} \\ -c & C & -c_{e\alpha} & -C_{e\alpha} & c_{ez} \\ C_{\alpha e} & c_{\alpha e} & C_\alpha & -c_\alpha & C_{e\alpha} \\ c_{\alpha e} & -C_{\alpha e} & c_\alpha & C_\alpha & C_{e\alpha} \\ C_{ze} & c_{ze} & C_{ze} & c_{ze} & C_z \end{bmatrix} \begin{bmatrix} \dot{X} \\ \dot{Y} \\ \dot{\alpha}_y \\ \dot{\alpha}_x \\ \dot{Z} \end{bmatrix}
$$

$$
+ \begin{bmatrix} K & k & K_{e\alpha} & -k_{e\alpha} & K_{ez} \\ -k & K & -k_{e\alpha} & -K_{e\alpha} & k_{ez} \\ K_{\alpha e} & k_{\alpha e} & K_\alpha & -k_\alpha & K_{e\alpha} \\ k_{\alpha e} & -K_{\alpha e} & k_\alpha & K_\alpha & k_{e\alpha} \\ K_{ze} & k_{ze} & K_{z\alpha} & k_{z\alpha} & K_z \end{bmatrix} \begin{bmatrix} X \\ Y \\ \alpha_y \\ \alpha_x \\ Z \end{bmatrix}
$$

FIGURE 1: Representation of the MDI forces by mass, damping and stiffness matrices
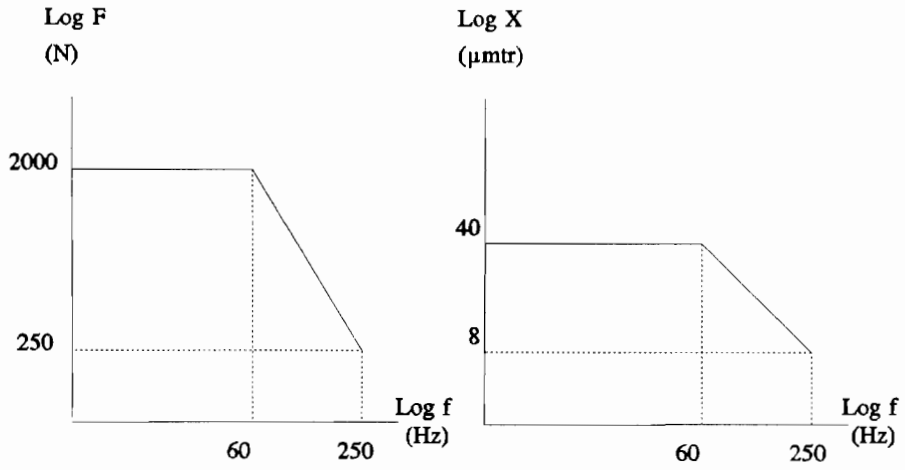
FIGURE 2: Artificial force and displacement spectrums
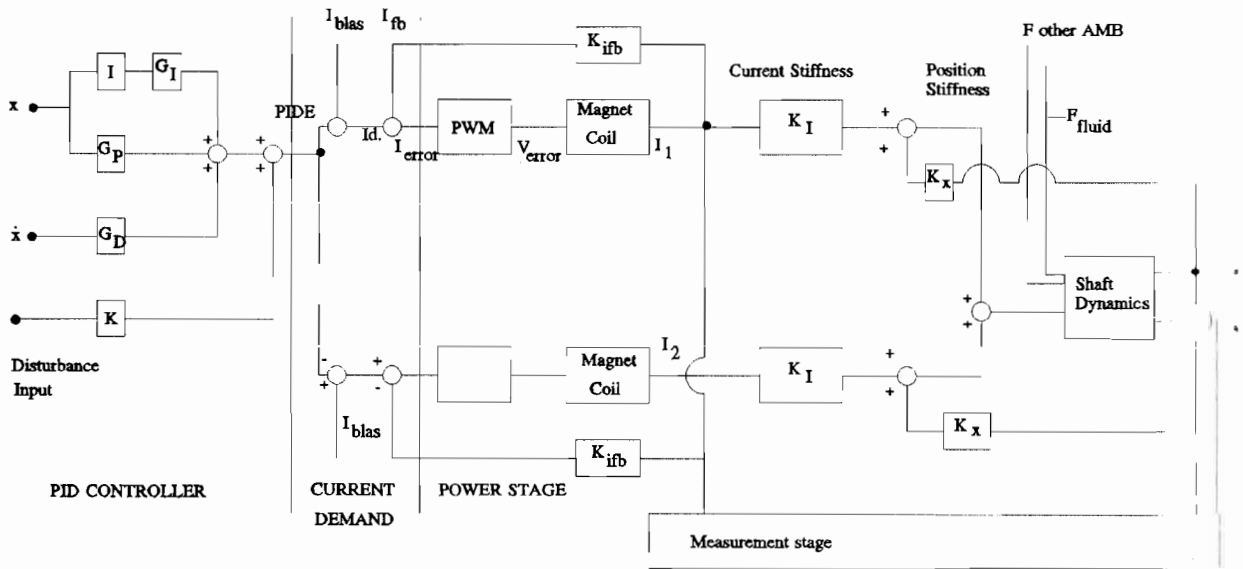
FIGURE 3: Controller scheme for 1 DOF magnetic bearing
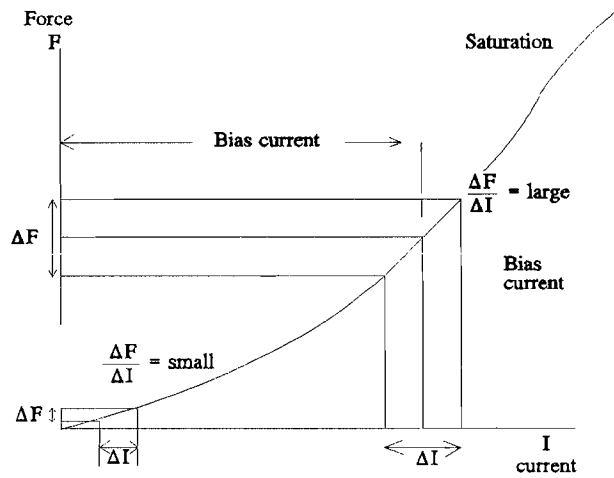
FIGURE 4: Control via current (ΔI)

SHAFT CENTER POSITION
INFLUENCE

50_micron_up

REFPOS

50_micron_down

FJ3:35:+X
FEXT:50:+X
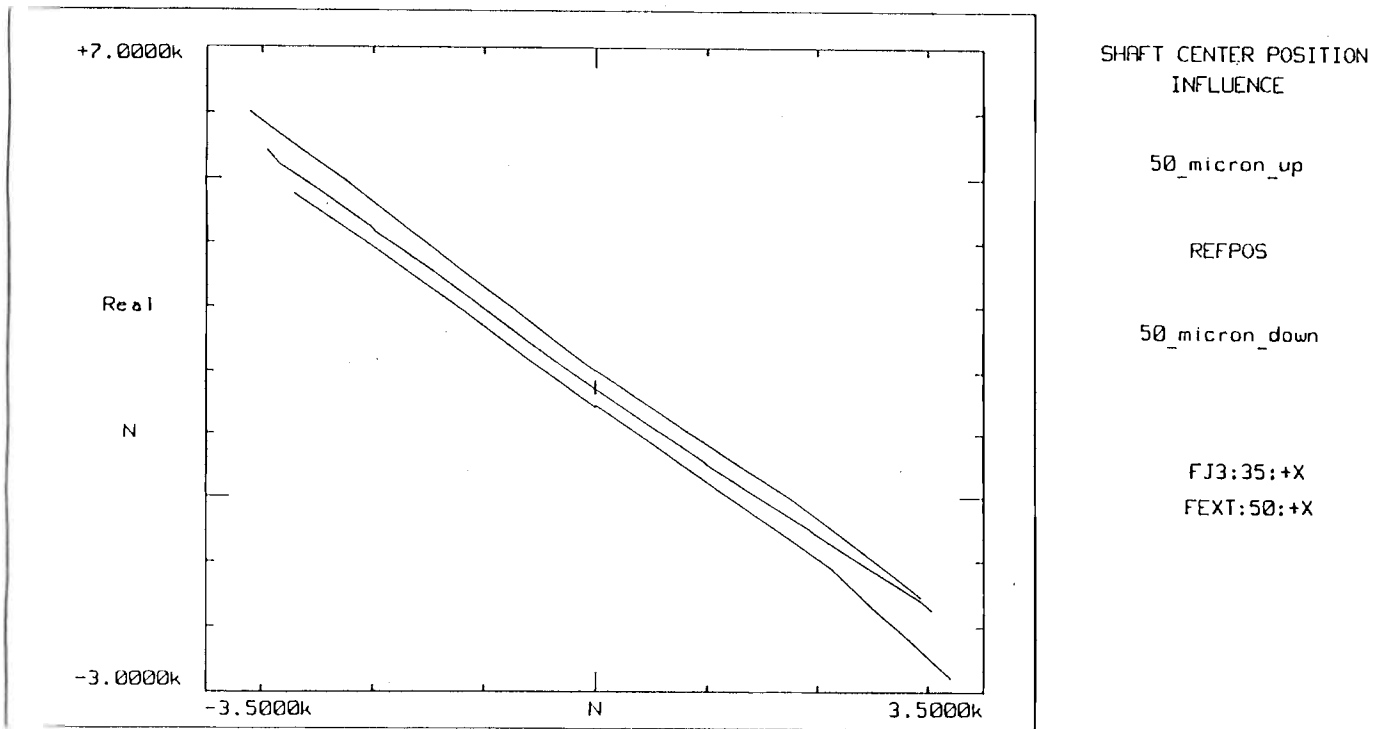
FIGURE 5: DC force calibration: dependency of the calculated force in the AMB on the position of the shaft centre

Check map J3 Force error.
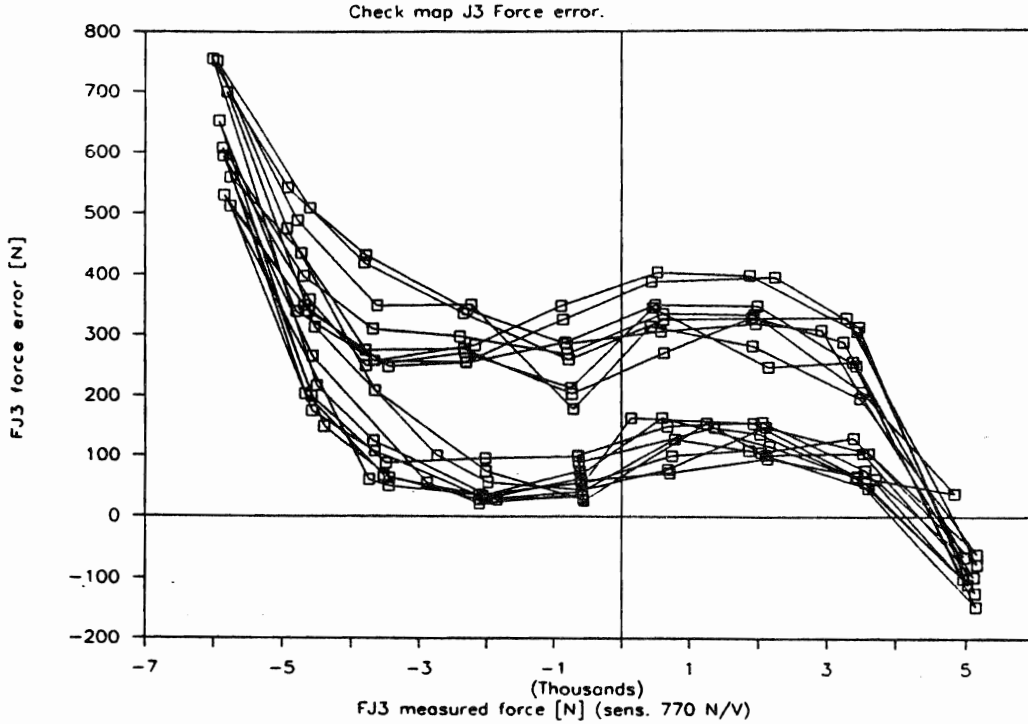
FIGURE 6: Residual force output error for vertical direction
From test rig University of Kaiserslautern
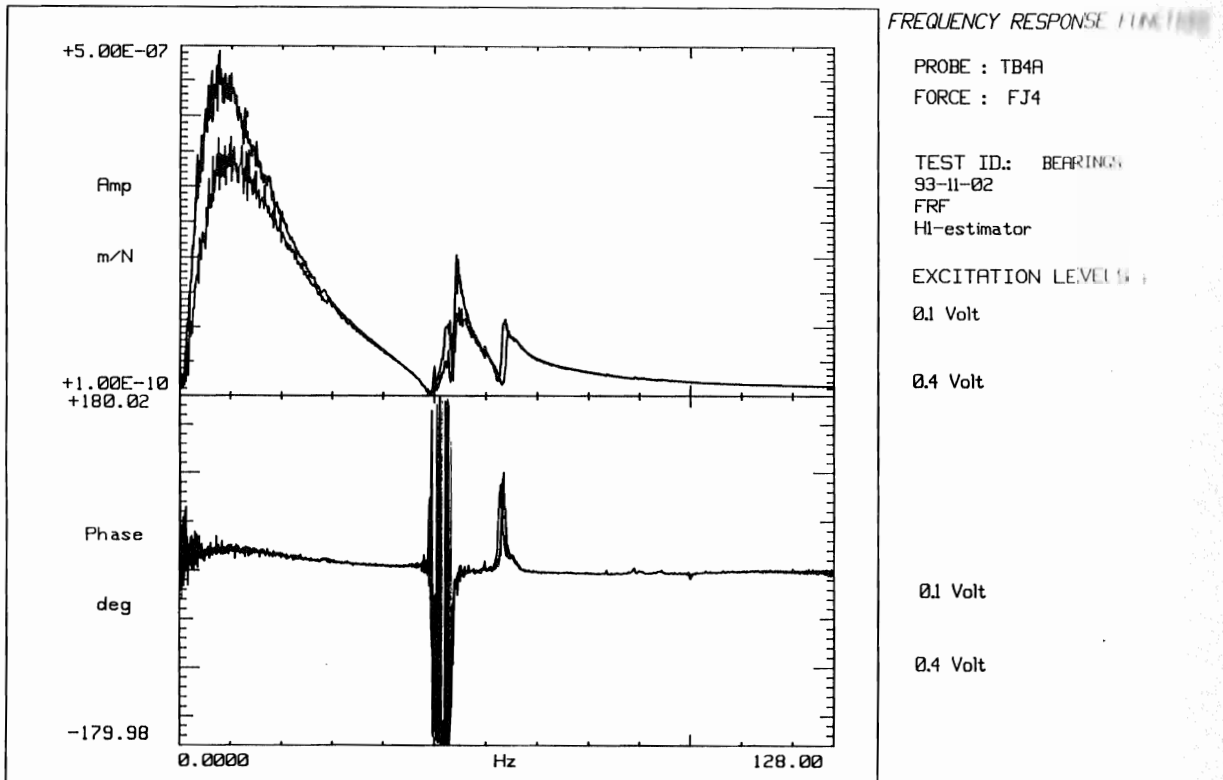
FIGURE 7a: Linearity check of bearings for 2 excitation levels.
Broad band excitation.
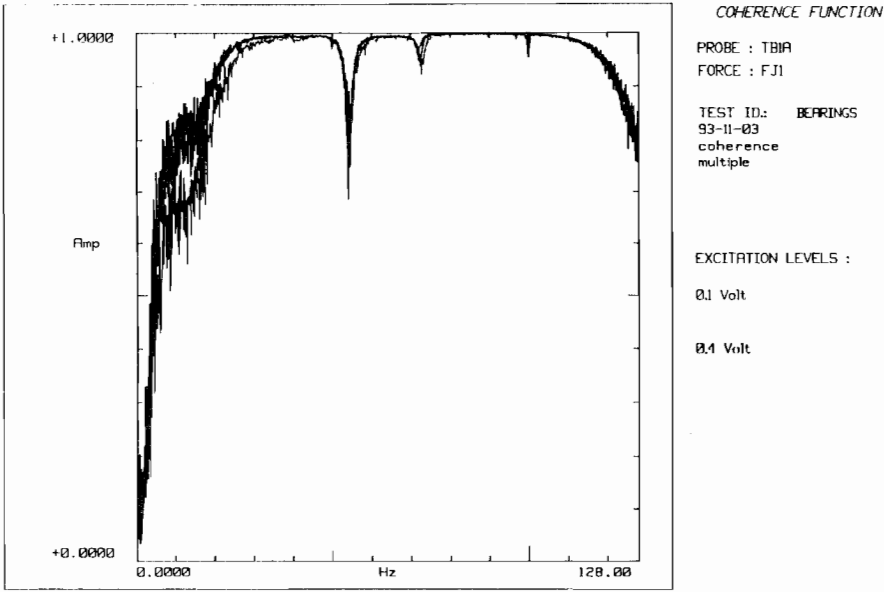
FIGURE 7b: Coherence for broad band excitation
Lower curve: 0.1 V. Upper curve: 0.4 V.
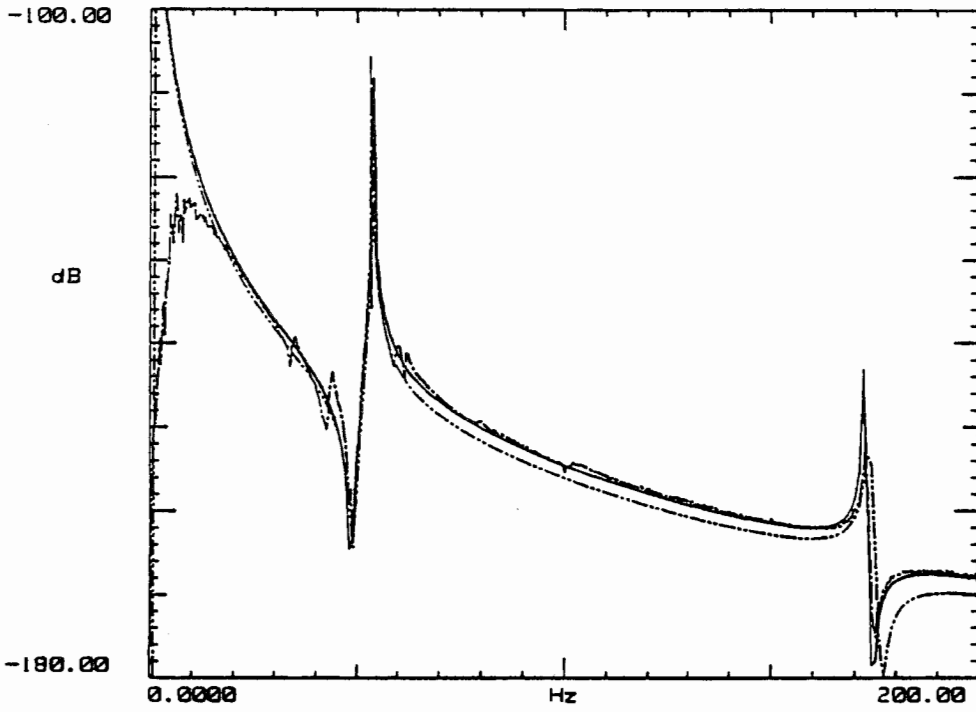
FIGURE 8: Comparison of measured and modelled FRF. Broadband excitation.
(-) Analytical model, (-.-) AMB excitation, (-..-..) Hammer excitation
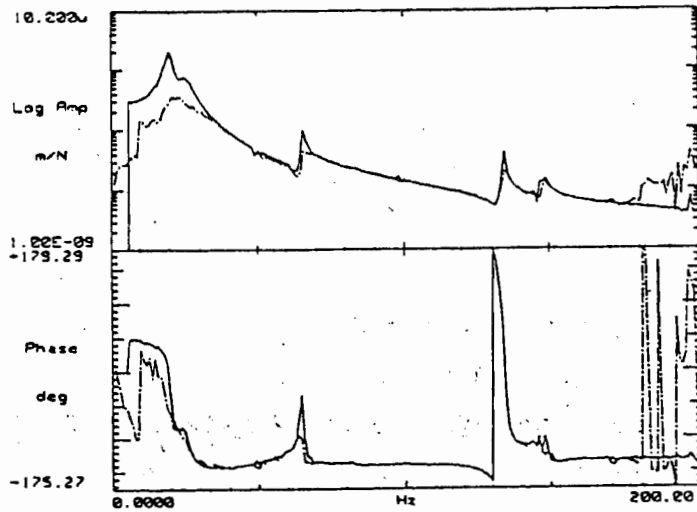
FIGURE 9a: STS (solid) and broadband (dash) measured FRF at outboard bearing
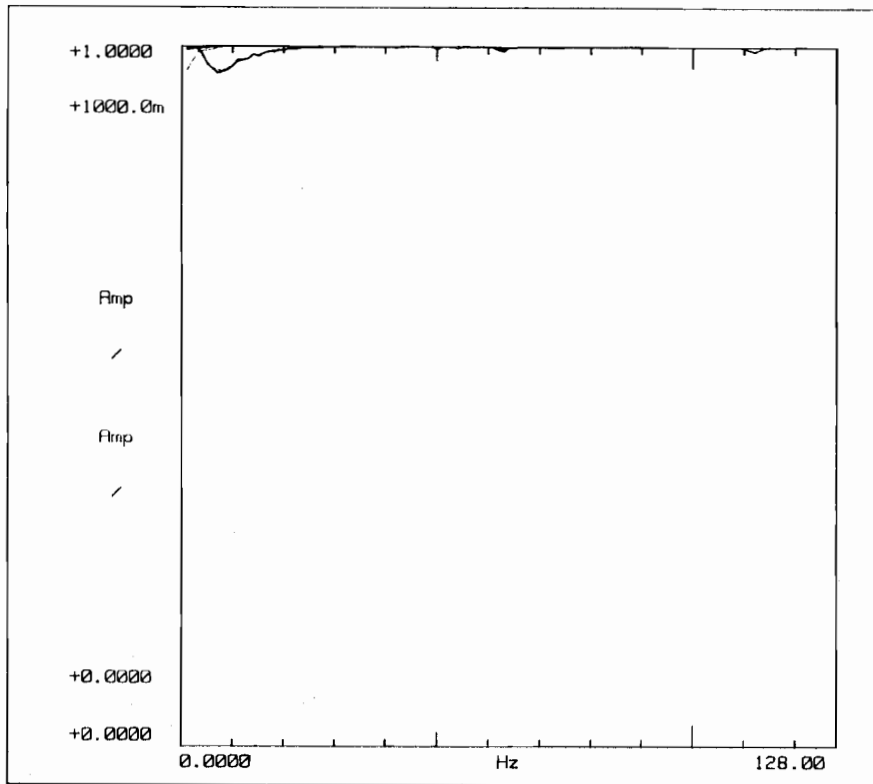
FIGURE 9b: Coherence for STS excitation

F1		F2		F3		F4		graphic representation	
A	ϕ	A	ϕ	A	ϕ	A	ϕ		
1	0	1	90	1	0	1	90		FW, radial
1	0	1	-90	1	0	1	-90		BW, radial
1	0	1	0	1	0	1	0		pure radial
1	0	1	90	1	180	1	270		FW conical
1	0	1	180	1	0	1	180		pure radial
1	0	1	270	1	180	1	90		BW conical

FIGURE 10: Multiple input force set for excitation of the rotor, in radial direction
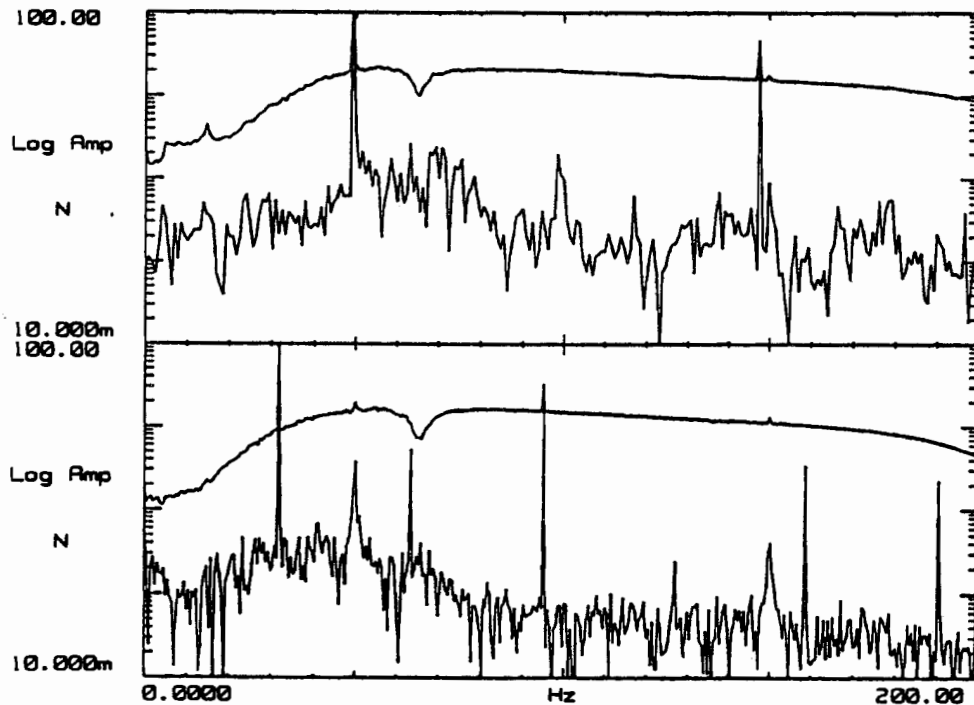
FIGURE 11a: A force spectrum with and without excitation for different speeds. The upper graph corresponds to 2950 rpm, the lower graph is measured at 1900 rpm.
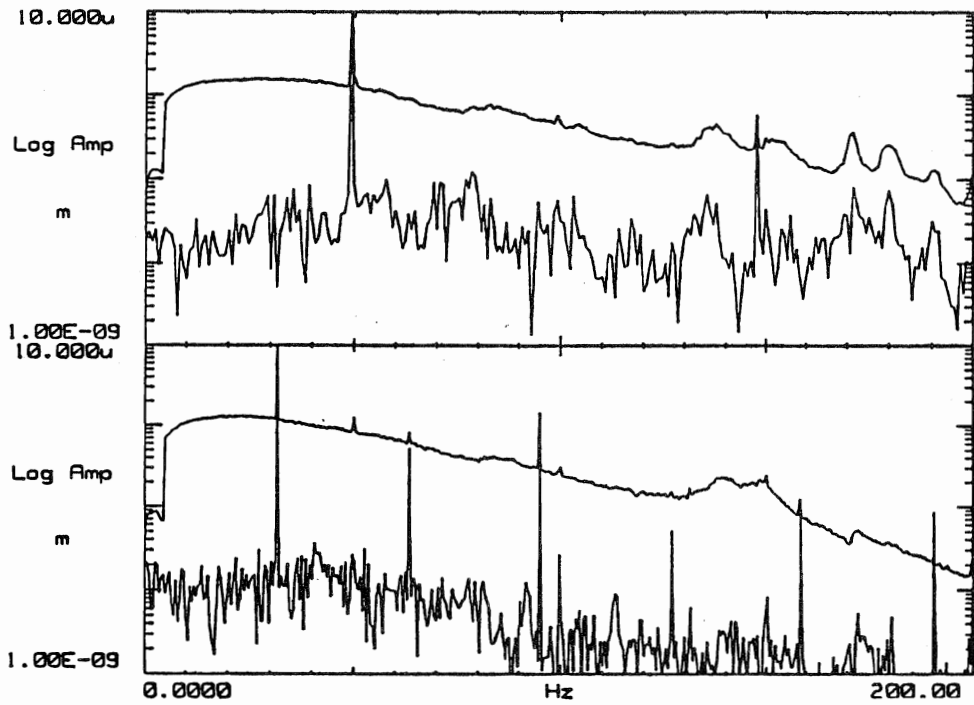
FIGURE 11b: Displacement spectrum with and without excitation for different speeds. The upper graph corresponds to 2950 rpm, the lower graph is measured at 1900 rpm
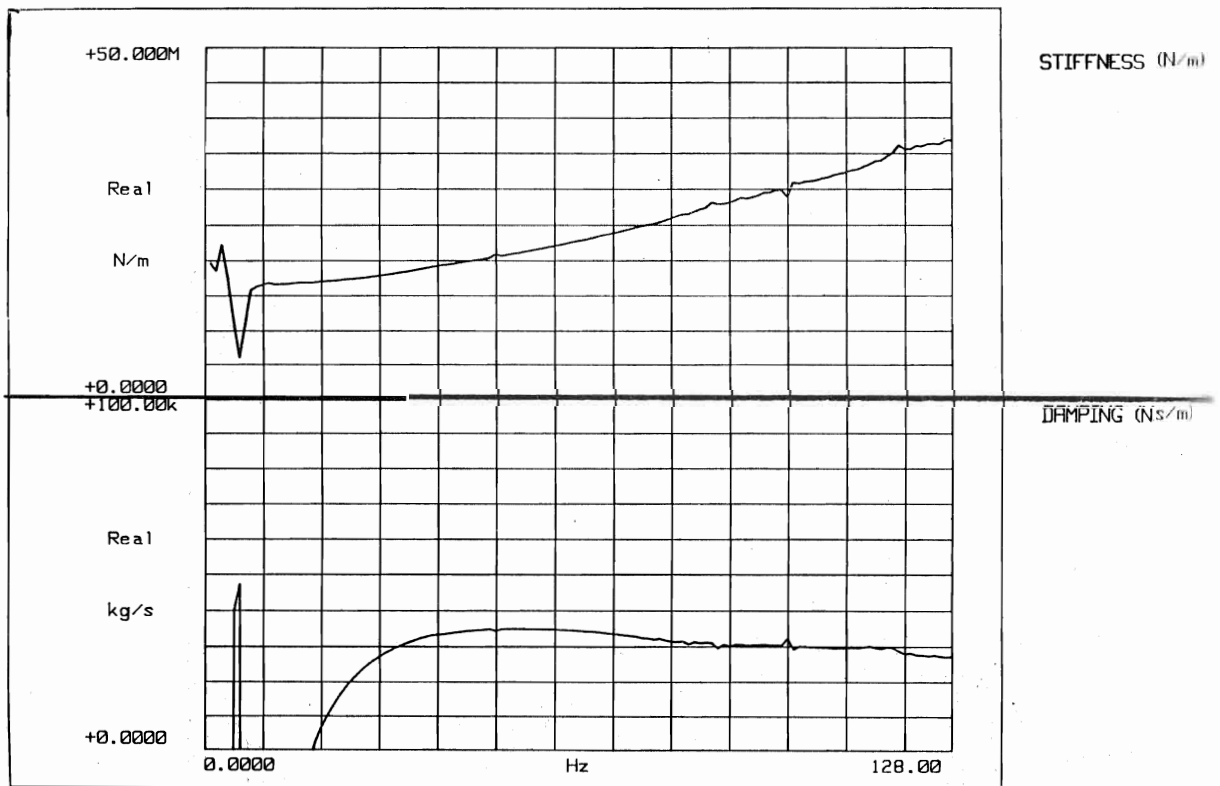
FIGURE 12: Equivalent stiffness (upper part) and damping (lower part) of the inboard bearing - vertical direction
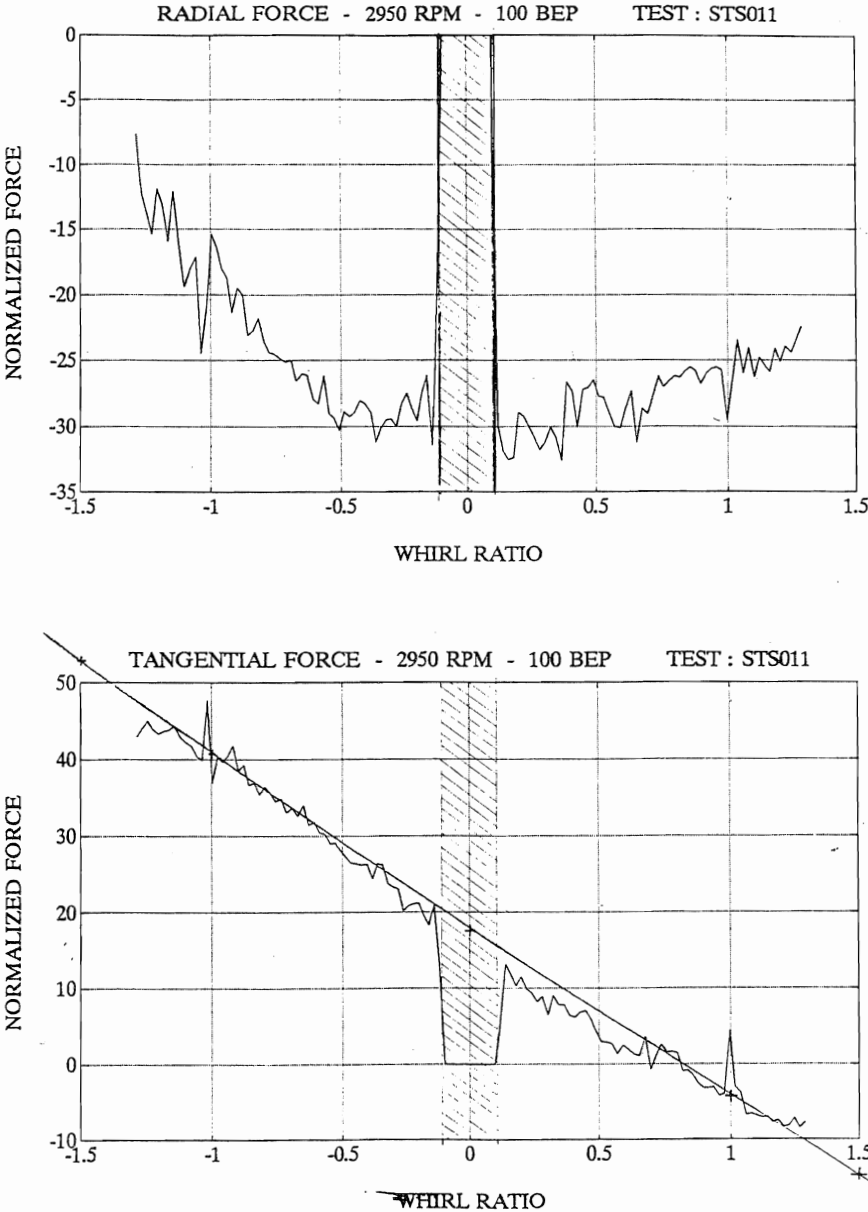
FIGURE 13: Radial and tangential MDI forces of a centrifugal impeller identified by AMB excitation